grins containing mutations that abrogate talin binding [β3(L746A) or β3(W739A)] exhibited reduced PAC-1 binding (Fig. 4C). In contrast, point mutations in the β3 tail that did not interfere with talin binding did not affect PAC-1 binding. Anti-LIBS6 increased PAC-1 binding to all the mutant integrins, regardless of their ability to bind talin (Fig. 4C). Similar results were observed for αIIbα6Aβ3, αIIbα6Bβ3, and αIIbβ3 integrins (Fig. 4D). However, the energy-independent activated state of αIIbαLΔβ3 was not affected by β3 mutations (Fig. 4E). Thus, talin binding to integrin β tails is required for cellular activation of integrins.

We also generated point mutations within the talin PTB-like domain that reduce binding to β3 tails (R358A, W359A, and A360E) and one mutation that does not (K357A) (*13*, *19*). When expressed in CHO cells, only the wild-type and K357A talin fragments stimulated PAC-1 binding to αIIbβ3, whereas talin fragments containing mutations that disrupt integrin binding did not (Fig. 4F). In all cases, anti-LIBS6 stimulated PAC-1 binding, confirming that αIIbβ3 was still expressed and could be activated externally (*13*). Thus, talin is required for integrin activation, and mutations within the talin PTB-like domain that prevent integrin β tail binding block its ability to induce integrin activation.

We have established that talin binding to integrin β tails is the final step leading to integrin activation. Regulation of this step, perhaps by phosphorylation (*21*), proteolysis (*22*), or phosphoinositide binding (*23*), may be a final common element in signaling pathways that control integrin activation. Although integrin residues critical for talin binding are localized within the W739 to K748 region, membrane-proximal β3 tail residues are also perturbed upon binding of activating fragments of talin (*19*, *24*). Associations between the membrane-proximal regions of α and β tails are thought to prevent integrin activation (*3*, *9*, *24*, *25*), and talin binding may induce integrin activation by disrupting their interaction (*24*). Deletion of the membrane-proximal regions generates integrins that remain activated in the absence of talin or metabolic energy (*10*). Therefore, talin-integrin interactions mediate integrin activation, possibly through effects on the membrane-proximal regions of integrin β tails.

References and Notes

1. S. P. Palecek, J. C. Loftus, M. H. Ginsberg, A. F. Horwitz, D. A. Lauffenburger, *Nature* **385**, 537 (1997).
2. C. Wu, V. M. Keivens, T. E. O'Toole, J. A. McDonald, M. H. Ginsberg, *Cell* **83**, 715 (1995).
3. R. O. Hynes, *Cell* **110**, 673 (2002).
4. D. A. Calderwood *et al.*, *J. Biol. Chem.* **274**, 28071 (1999).
5. Materials and methods are available as supporting material on *Science* Online.
6. T. E. O'Toole *et al.*, *Science* **254**, 845 (1991).
7. P. J. Paddison, A. A. Caudy, E. Bernstein, G. J. Hannon, D. S. Conklin, *Genes Dev.* **16**, 948 (2002).
8. A. L. Frelinger III, X. Du, E. F. Plow, M. H. Ginsberg, *J. Biol. Chem.* **266**, 17106 (1991).
9. P. E. Hughes *et al.*, *J. Biol.Chem.* **271**, 6571 (1996).
10. T. E. O'Toole *et al.*, *J. Cell Biol.* **124**, 1047 (1994).
11. T. Hato, N. Pampori, S. J. Shattil, *J. Cell Biol.* **141**, 1685 (1998).
12. N. Pampori *et al.*, *J. Biol. Chem.* **274**, 21609 (1999).
13. S. Tadokoro *et al.*, data not shown.
14. K. Eto *et al.*, *Proc. Natl. Acad. Sci. U.S.A.* **99**, 12819 (2002).
15. H. Kashiwagi *et al.*, *J. Cell Biol.* **137**, 1433 (1997).
16. T. Sethi, M. H. Ginsberg, J. Downward, P. E. Hughes, *Mol. Biol. Cell* **10**, 1799 (1999).
17. C. A. Fenczik, T. Sethi, J. W. Ramos, P. E. Hughes, M. H. Ginsberg, *Nature* **390**, 81 (1997).
18. D. A. Calderwood *et al.*, *J. Biol. Chem.* **277**, 21749 (2002).
19. B. Garcia-Alvarez *et al.*, *Mol. Cell* **11**, 49 (2003).
20. D. A. Calderwood, S. J. Shattil, M. H. Ginsberg, *J. Biol. Chem.* **275**, 22607 (2000).
21. P. Tapley, A. Horwitz, C. A. Buck, K. Duggan, L. Rohrschneider, *Oncogene* **4**, 325 (1989).
22. B. Yan, D. A. Calderwood, B. Yaspan, M. H. Ginsberg, *J. Biol. Chem.* **276**, 28164 (2001).
23. V. Martel *et al.*, *J. Biol. Chem.* **276**, 21217 (2001).
24. O. Vinogradova *et al.*, *Cell* **110**, 587 (2002).
25. J. Takagi, B. M. Petre, T. Walz, T. A. Springer, *Cell* **110**, 599 (2002).

26. Supported by grants from the NIH and American Heart Association.

Supporting Online Material

www.sciencemag.org/cgi/content/full/302/5642/103/DC1
Materials and Methods
Figs. S1 to S3
References

9 May 2003; accepted 21 August 2003

Self-Assembly of Proteins into Designed Networks

Philippe Ringler and Georg E. Schulz*

A C_4-symmetric tetrameric aldolase was used to produce a quadratic network consisting of the enzyme as a rigid four-way connector and stiff streptavidin rods as spacers. Each aldolase subunit was furnished with a His_6 tag for oriented binding to a planar surface and two tethered biotins for binding streptavidin in an oriented manner. The networks were improved by starting with composite units and also by binding to nickel–nitrilotriacetic acid–lipid monolayers. The mesh was adjustable in 5-nanometer increments. The production of a net with switchable mesh was initiated with the use of a calcium ion–containing β-helix spacer that denatured on calcium ion depletion.

The production of a designed arrangement of matter at the molecular level is a central goal of contemporary engineering endeavors (*1*). Besides micropositioning strategies (*2*, *3*), the materials can also be placed by spontaneous self-assembly processes (*4*). Efficient biological self-assembly systems are, for instance, myosin filaments, the large heterocomplex ribosome, bacterial S layers (*5*), and membranes containing two-dimensional arrays of bacteriorhodopsin (*6*) or porins (*7*). Novel assemblies can be designed and produced with the use of engineered biological building blocks (*5*, *8*–*11*). Molecular assemblies may be desiccated and then viewed by transmission electron microscopy or followed in situ with an atomic force microscope (*12*, *13*). Here, we report a noncovalent planar network consisting of two biologically unrelated proteins and show how the mesh can be adjusted and also made switchable by varying the Ca^{2+} concentration.

We chose the structurally characterized proteins L-rhamnulose-1-phosphate aldolase (RhuA) and streptavidin as building blocks. RhuA is a C_4-symmetric tetramer consisting of 274 amino acid residues per subunit (*14*). It resembles a flattened cube with dimensions of 7 nm by 7 nm by 5 nm. Streptavidin is a D_2-symmetric tetramer with 159 residues and one biotin-binding site per subunit (*15*, *16*). It forms a brick with dimensions of 6 nm by 5 nm by 4 nm and a pair of biotin-binding sites on each of the two 6-nm-by-4-nm faces (Fig. 1A). RhuA was fused with a His_6 tag at each of the four C termini protruding from the top face, which was essential for the assembly on a lipid monolayer and for all purification steps.

In order to fasten two tethered biotins at each side face of RhuA at positions that would connect to juxtaposed biotin-binding sites of streptavidin, we introduced the mutations $Asn^{133} \rightarrow Cys^{133}$, $Lys^{261} \rightarrow Cys^{261}$, and $Cys^{126} \rightarrow Ser^{126}$ (C126S) (*17*, *18*). The C126S mutation was necessary for the removal of an interfering thiol. The cysteines were labeled with tethered biotin (*18*), giving rise to building block ^{b}R carrying eight biotins (Fig. 1A). The tethers were short enough to prevent streptavidin (S) binding on a corner so that ^{b}R acted as a rigid four-way connector, binding block S only at its side faces.

Institut für Organische Chemie und Biochemie, Albert-Ludwigs-Universität Freiburg, Albertstrasse 21, D-79104 Freiburg im Breisgau, Germany.

*To whom correspondence should be addressed. E-mail: schulz@bio.chemie.uni-freiburg.de

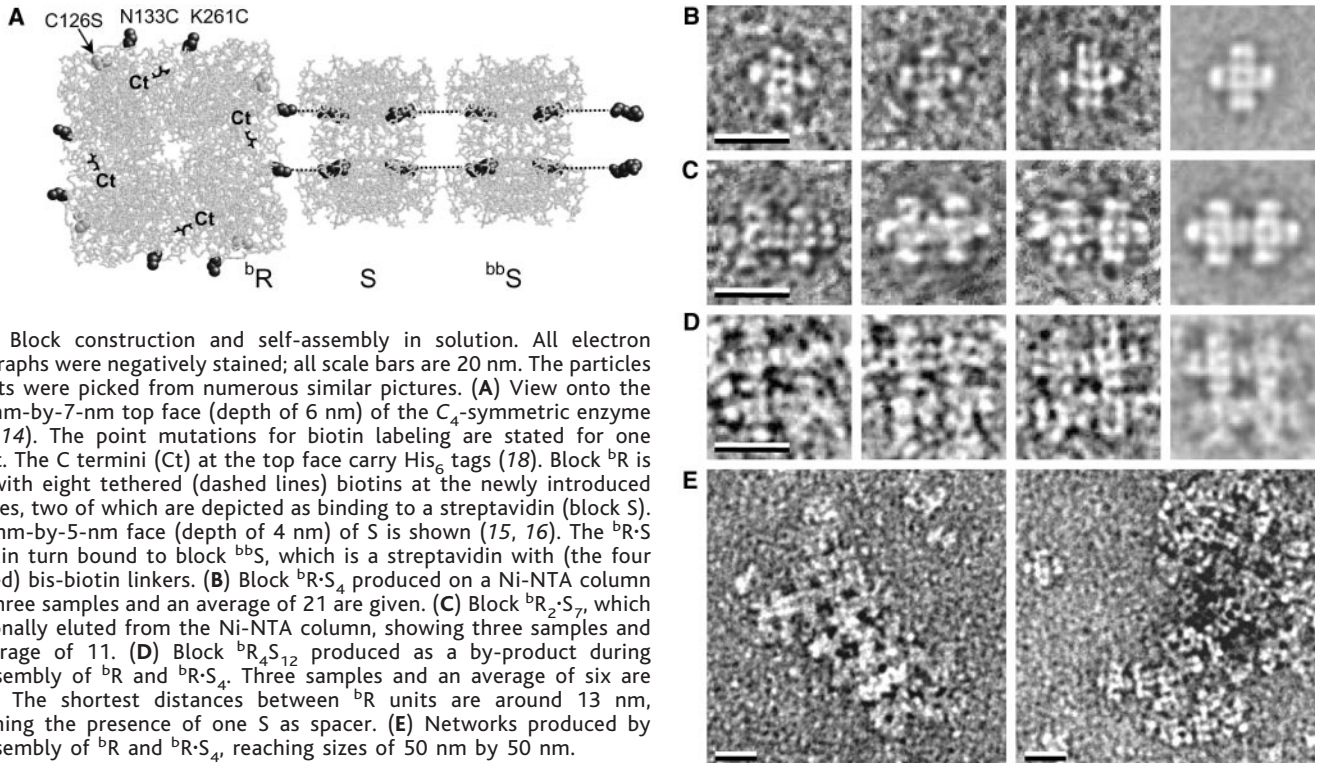

Fig. 1. Block construction and self-assembly in solution. All electron micrographs were negatively stained; all scale bars are 20 nm. The particles and nets were picked from numerous similar pictures. (**A**) View onto the flat 7-nm-by-7-nm top face (depth of 6 nm) of the C_4-symmetric enzyme RhuA (*14*). The point mutations for biotin labeling are stated for one subunit. The C termini (Ct) at the top face carry His_6 tags (*18*). Block ^{b}R is RhuA with eight tethered (dashed lines) biotins at the newly introduced cysteines, two of which are depicted as binding to a streptavidin (block S). The 6-nm-by-5-nm face (depth of 4 nm) of S is shown (*15*, *16*). The $^{b}R{\cdot}S$ unit is in turn bound to block ^{bb}S, which is a streptavidin with (the four depicted) bis-biotin linkers. (**B**) Block $^{b}R{\cdot}S_4$ produced on a Ni-NTA column (*18*). Three samples and an average of 21 are given. (**C**) Block $^{b}R_2{\cdot}S_7$, which occasionally eluted from the Ni-NTA column, showing three samples and an average of 11. (**D**) Block $^{b}R_4S_{12}$ produced as a by-product during self-assembly of ^{b}R and $^{b}R{\cdot}S_4$. Three samples and an average of six are shown. The shortest distances between ^{b}R units are around 13 nm, confirming the presence of one S as spacer. (**E**) Networks produced by self-assembly of ^{b}R and $^{b}R{\cdot}S_4$, reaching sizes of 50 nm by 50 nm.

Equimolar mixtures of the building blocks ^{b}R and S in solution showed a strong tendency to form large globular aggregates. Therefore, we produced and purified the building block $^{b}R{\cdot}S_4$, ^{b}R decorated with one S at each of its side faces (Fig. 1B). The planar $^{b}R{\cdot}S_4$ then presents four pairs of biotin-binding sites that can be occupied by the tethered biotins of ^{b}R blocks. $^{b}R{\cdot}S_4$ was prepared by rapidly mixing a solution of 2 μM ^{b}R with an eightfold molar excess of S. Rapid mixing was expected to reduce crosslinking into larger aggregates. Excess S and large aggregates were removed on a Ni–nitrilotriacetic acid (NTA) column. The eluate was analyzed by electron microscopy and revealed the expected $^{b}R{\cdot}S_4$ block but also $^{b}R{\cdot}S_4{\cdot}^{b}R{\cdot}S_3$ dimers and some higher aggregates (Fig. 1, B and C).

In a first self-assembly experiment, equimolar amounts of $^{b}R{\cdot}S_4$ and ^{b}R were mixed in solution. Electron micrographs of the mixture revealed a collection of small planar quadratic nets where the distance between two ^{b}R molecules was 13 nm, which is in the expected range for a single streptavidin spacer (Fig. 1D). However, the network sizes did not exceed 50 nm by 50 nm, as shown in Fig. 1E, presumably because irregularities arose from insufficiently labeled ^{b}R (*18*).

In a second experiment, a monolayer of the lipid Ni-2-(bis-carboxymethyl-amino)-6-[2-(1,3)-di-*O*-oleyl-glyceroxy)-acetyl-amino] hexanoic acid (Ni-NTA-DOGA) (*18*–*20*) diluted in dioleoyl phosphatidylcholine was spread on the surface of a solution containing building block $^{b}R{\cdot}S_4$ (*18*). A small volume of an ^{b}R solution was then injected below the surface of the lipid film. After overnight incubation, the lipid monolayer with the interacting proteins was transferred to a carbon grid and negatively stained. The resulting electron micrographs showed patterns that resembled a woven fabric with the expected mesh size (Fig. 2). The network extended over more than 200 nm, in contrast to the 50-nm patches observed in the lipid-free approach, indicating that the planar monolayer indeed facilitated the formation of the planar network.

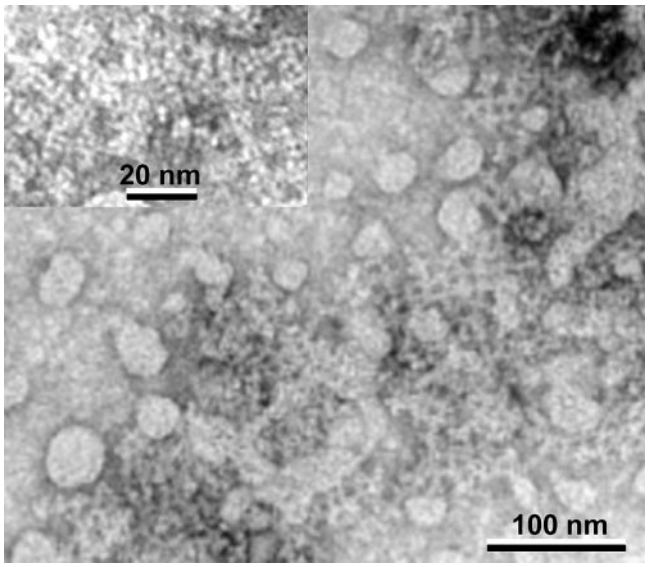

Fig. 2. Representative negatively stained example of the networks formed by self-assembly of blocks ^{b}R and $^{b}R{\cdot}S_4$ at a lipid monolayer. The lattices extend over more than 200 nm by 200 nm but contain irregularities. (**Insert**) A magnified sample.

The mesh was then extended by incubating the building block $^{b}R{\cdot}S_4$ with bis-biotin-labeled streptavidin (^{bb}S) produced as described (*18*). The result was analyzed by electron microscopy. Besides large disordered aggregates, we observed a collection of four-unit nets with an ^{b}R-to-^{b}R distance of 20 nm (Fig. 3A), confirming the expected $S{\cdot}^{bb}S{\cdot}S$ spacer. For $^{b}R{\cdot}S_4$ bound to a Ni-NTA column, the steps of loading with ^{bb}S, washing, loading with S, and washing can be repeated, resulting in the defined species $^{b}R{\cdot}[S{\cdot}(^{bb}S{\cdot}S)_n]_4$ or $^{b}R{\cdot}[(S{\cdot}^{bb}S)_m]_4$ (where n and m are 0, 1, 2...) so that any uneven-numbered streptavidin spacer can be pro-

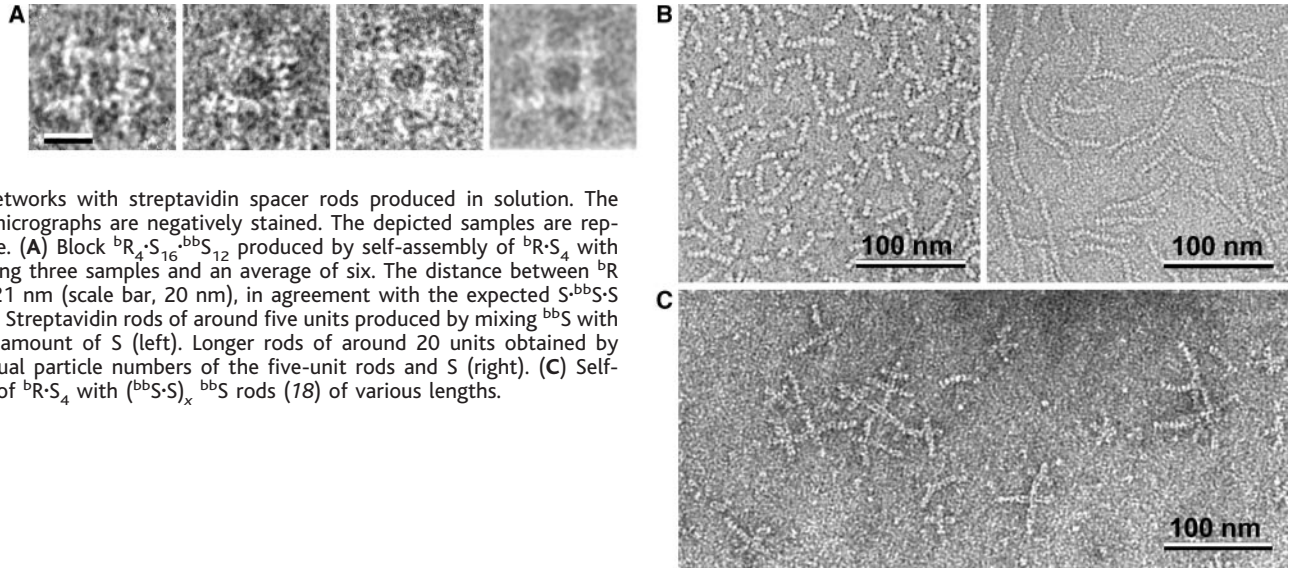

Fig. 3. Networks with streptavidin spacer rods produced in solution. The electron micrographs are negatively stained. The depicted samples are representative. (**A**) Block ${}^{b}R_4{\cdot}S_{16}{\cdot}{}^{bb}S_{12}$ produced by self-assembly of ${}^{b}R{\cdot}S_4$ with ${}^{bb}S$, showing three samples and an average of six. The distance between ${}^{b}R$ blocks is 21 nm (scale bar, 20 nm), in agreement with the expected $S{\cdot}{}^{bb}S{\cdot}S$ spacer. (**B**) Streptavidin rods of around five units produced by mixing ${}^{bb}S$ with a smaller amount of S (left). Longer rods of around 20 units obtained by mixing equal particle numbers of the five-unit rods and S (right). (**C**) Self-assembly of ${}^{b}R{\cdot}S_4$ with $({}^{bb}S{\cdot}S)_x$ ${}^{bb}S$ rods (*18*) of various lengths.

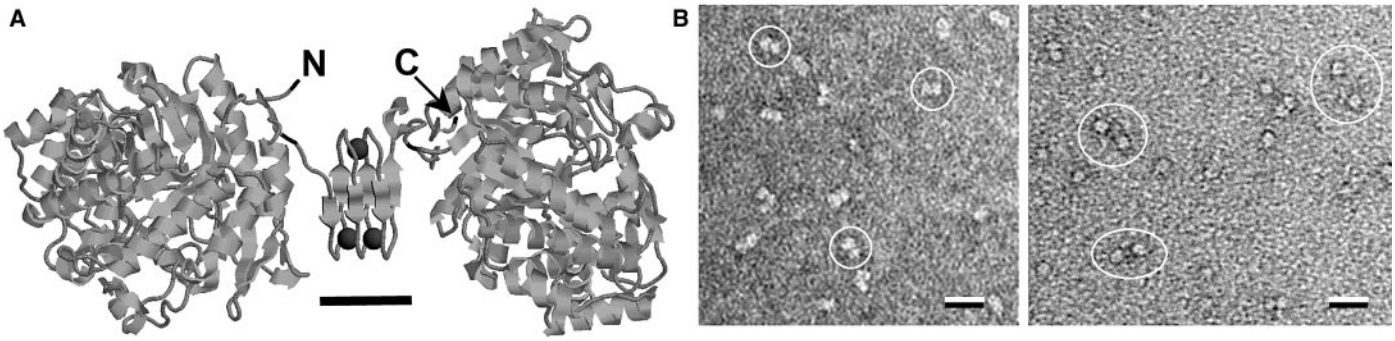

Fig. 4. The 998-residue construct PGAL-β-PGAL (*17*, *18*). (**A**) Ribbon model of the polypeptide indicating N and C termini of the construct. On Ca^{2+} removal, the β helix (scale bar, 2 nm) denatures, giving rise to a 20-nm peptide tether. (**B**) Electron micrographs of negatively stained solutions of PGAL-β-PGAL picked from numerous similar pictures (scale bars, 20 nm). The left side shows PGAL-β-PGAL after EDTA-free preparation (*22*), forming dumbbell-shaped particles (circled) corresponding to the model of (A). On the right side, the same preparation after treatment with 10 mM EDTA shows separated globular PGAL molecules (the denatured peptide is not visible).

duced by mixing with ${}^{b}R$ or ${}^{b}R{\cdot}S_4$, respectively. Even-numbered spacers are obtained if ${}^{b}R{\cdot}[S{\cdot}({}^{bb}S{\cdot}S)_n]_4$ blocks were bis-biotin-labeled as described for S (*18*) and then mixed with ${}^{b}R{\cdot}S_4$. Accordingly, the design allows spacer lengths of any multiple of 5 nm.

Furthermore, the mesh was increased by using less-well-defined streptavidin rods with ${}^{bb}S$ units at their ends. $({}^{bb}S{\cdot}S)_x{\cdot}{}^{bb}S$ rods with x ranging around 2 (Fig. 3B) were produced by mixing ${}^{bb}S$ with a smaller amount of S. After removing excess ${}^{bb}S$ by washing in a Centricon (Millipore, Bedford, MA) (100 kD cutoff), the remaining rods were again incubated with a small amount of S, which resulted in a length multiplication (Fig. 3B). The limited curvature of these rods indicates their stiffness. In turn, stiffness and the scarcity of branching points show that the internal tether of the applied bis-biotin (*18*) was of an appropriate length. These rods may find application as stiff spacers between any biotin- or streptavidin-labeled compounds. With ${}^{bb}S$ units at their ends, the rods can connect ${}^{b}R{\cdot}S_4$ blocks, forming large mesh networks. When ${}^{b}R{\cdot}S_4$ was incubated with rod distributions of various lengths, irregular planar networks were observed (Fig. 3C).

In order to design a protein lattice with a switchable mesh, we selected a Ca^{2+}-binding β-helix fragment of the enzyme serralysin from *Serratia marcescens* as a spacer (*21*). We assumed that this spacer would form a 2-nm solid rod with bound Ca^{2+} and would denature to a 20-nm mobile tether on Ca^{2+} removal by ethylenediaminetetraacetic acid (EDTA) (Fig. 4A). The fragment comprised three β-helix turns containing five times the characteristic motif GGxGxDxUx, where G is Gly, x is an arbitrary amino acid residue, D is Asp, and U is a large aliphatic residue. The first six residues of the motifs are involved in Ca^{2+} binding. In principle, this spacer can be infinitely extended by adding further repeats.

The concept was tested with the 998-residue tandem fusion protein PGAL-β-PGAL consisting of the globular monomeric 468-residue protein 6-phospho-β-galactosidase (PGAL) (*22*) and the β helix (*17*, *18*). The gene was expressed in *Escherichia coli* and purified as described (*22*). The product was analyzed by electron microscopy, showing dumbbell-shaped particles of the expected size that indicated that the spacer was short and presumably contained Ca^{2+} (Fig. 4B). After Ca^{2+} was removed with 10 mM EDTA, the electron micrographs showed pairs of particles at distances from 3 to 13 nm, which agrees with the expected distance distribution of random 20-nm coils (Fig. 4B). We conclude that EDTA had removed the Ca^{2+} ions and thus extended the spacer. Such a β-helix spacer may be used in future constructions, for instance by replacing the streptavidin linkers in the ${}^{b}R$ networks described above.

The designed planar networks of engineered proteins extend the two-dimensional supramolecular chemistry (*23*) to the realm of proteins. They follow extensive studies on DNA networks, making use of the recognition property of complementary single-stranded DNA (*24*). Compared with DNA, the proteins permit stiffer network elements and stronger associations. However, the strong binding of biotin to streptavidin (K_D equals 10^{-15} M) prevents self-healing of irregular lattice points as occurs, for instance,

during crystallization processes. This renders network assembly rather sensitive to inhomogeneities of the building blocks, which we experienced with respect to biotin-labeling of the cysteines of ^{b}R (*18*). Both problems may be ameliorated in future developments. Protein networks are well suited to placing functional proteins such as enzymes or membrane channels at defined relative positions, because such functions can be conveniently added by protein fusions (*18*). This may improve contemporary molecular lithography (*25*). Moreover, it permits the construction of spatially ordered biochemical teams, which may also include membrane components (*26*).

References and Notes

1. K. E. Drexler, *Trends Biotechnol.* **17**, 5 (1999).
2. R. D. Piner, J. Zhu, F. Xu, S. Hong, C. A. Mirkin, *Science* **283**, 661 (1999).
3. P. Morales *et al.*, *Mater. Sci. Eng. C* **2**, 173 (1995).
4. G. M. Whitesides, M. Boncheva, *Proc. Natl. Acad. Sci. U.S.A.* **99**, 4769 (2002).
5. U. B. Sleytr *et al.*, *Progr. Colloid Polym. Sci.* **121**, 57 (2002).
6. R. Henderson, P. N. T. Unwin, *Nature* **257**, 28 (1975).
7. J. P. Chalcroft, H. Engelhardt, W. Baumeister, *FEBS Lett.* **211**, 53 (1987).
8. R. F. Service, *Science* **298**, 2322 (2002).
9. J. E. Padilla, C. Colovos, T. O. Yeates, *Proc. Natl. Acad. Sci. U.S.A.* **98**, 2217 (2001).
10. T. O. Yeates, J. E. Padilla, *Curr. Opin. Struct. Biol.* **12**, 464 (2002).
11. N. Dotan, D. Arad, F. Frolow, A. Freeman, *Angew. Chem. Int. Ed.* **38**, 2363 (1999).
12. S. Scheuring, D. J. Müller, P. Ringler, J. B. Heymann, A. Engel, *J. Microsc.* (Oxford) **193**, 28 (1999).
13. I. Reviakine, W. Bergsma-Schutter, A. Brisson, *J. Struct. Biol.* **121**, 356 (1998).
14. M. Kroemer, G. E. Schulz, *Acta Crystallogr.* **D58**, 824 (2002).
15. W. A. Hendrickson, *et al.*, *Proc. Natl. Acad. Sci. U.S.A.* **86**, 2190 (1989).
16. P. C. Weber, D. H. Ohlendorf, J. J. Wendoloski, F. R. Salemme, *Science* **243**, 85 (1989).
17. The plasmid is available on request.
18. Experimental details are given as supporting material on *Science* Online.
19. N. Bischler *et al.*, *Biophys. J.* **74**, 1522 (1998).
20. C. Richard, F. Balavoine, P. Schultz, T. W. Ebbesen, C. Mioskowski, *Science* **300**, 775 (2003).
21. U. Baumann, *J. Mol. Biol.* **242**, 244 (1994).
22. C. Wiesmann, G. Beste, W. Hengstenberg, G. E. Schulz, *Structure* **3**, 961 (1995).
23. J. Michl, T. F. Magnera, *Proc. Natl. Acad. Sci. U.S.A.* **99**, 4788 (2002).
24. N. C. Seeman, *Nature* **421**, 427 (2003).
25. K. Keren *et al.*, *Science* **297**, 72 (2002).
26. P. Ringler, G. E. Schulz, *ChemBioChem*, 463 (2002).

27. We thank P. Schultz (Institut de Génétique et de Biologie Moléculaire et Cellulaire, Illkirch, France) for a gift of the nickel-chelating lipid. The project was supported by the Deutsche Forschungsgemeinschaft under SFB-428.

Supporting Online Material

www.sciencemag.org/cgi/content/full/302/5642/106/DC1
Materials and Methods
Figs. S1 to S3
References and Notes

16 June 2003; accepted 20 August 2003

Untangling Desmosomal Knots with Electron Tomography

Wanzhong He,[1] Pamela Cowin,[2] David L. Stokes[1,2,3]*

Cell adhesion by adherens junctions and desmosomes relies on interactions between cadherin molecules. However, the molecular interfaces that define molecular specificity and that mediate adhesion remain controversial. We used electron tomography of plastic sections from neonatal mouse skin to visualize the organization of desmosomes in situ. The resulting three-dimensional maps reveal individual cadherin molecules forming discrete groups and interacting through their tips. Fitting of an x-ray crystal structure for C-cadherin to these maps is consistent with a flexible intermolecular interface mediated by an exchange of amino-terminal tryptophans. This flexibility suggests a novel mechanism for generating both cis and trans interactions and for propagating these adhesive interactions along the junction.

Two major types of intercellular adhesive junctions, desmosomes and adherens junctions, maintain cell shape and tissue integrity. Adherens junctions initiate cell contact and are found as adhesive belts, patches, and puncta between a wide variety of cells (*1–3*). Desmosomes reinforce and sustain adhesion and are particularly prevalent in organs subject to shear stress, such as heart and skin (*4*). Both enhance torsional strength by linking to the cytoskeleton. The physiological importance of cellular adhesion is illustrated by genetic and autoimmune diseases associated with various junctional components and by the phenotypes of their genetic knockout in mice. In particular, defects in desmosomal proteins disrupt heart, skin, and hair (*4, 5*), whereas those affecting proteins of the adherens junction increase cell proliferation and migration and are thus associated with carcinogenesis and metastasis (*6*).

Despite a distinct molecular composition, desmosomes and adherens junctions adopt a similar architectural strategy. Both types of junctions use physical associations between members of the cadherin family of calcium-dependent cell adhesion molecules, whose cytoplasmic domains are tethered to the cytoskeleton via an electron-dense plaque of intracellular proteins. Desmosomes contain two types of cadherins, desmoglein and desmocollin, whereas adherens junctions comprise a single type of classical cadherin (*7, 8*). Desmosomal and classical cadherins belong to the most closely related branches of the cadherin superfamily (*9*) and are characterized by the presence of five tandem, independently folding extracellular domains (EC1 to EC5) that each contain the highly conserved calcium-binding motifs Asp-X-Asp, Leu-Asp-Arg-Glu, and Asp-X-Asn-Asp-Asn (*10*). The x-ray structures of several classical cadherins (E, N, and C) show that all EC domains adopt a β sandwich related to the immunoglobulin fold, with calcium ions bound to the loops joining individual domains (*11, 12*). Desmosomal cadherins are very likely to have analogous structures given their high sequence similarity (*13*), including the conserved pattern of Pro, Gly, and hydrophobic residues that define the immunoglobulin fold (*14–16*).

Considerable interest has focused on identifying molecular interfaces that mediate the association of classical cadherins. Mutational studies as well as adhesion-inhibitory antibodies and peptides have implicated EC1 domains, in particular Trp[2] and the region of the conserved His-Ala-Val (HAV) sequence (*17–22*). X-ray crystallography has shown this N-terminal Trp to insert into a pocket formed by hydrophobic residues in the vicinity of the HAV sequence. In the initial structure, a dimer resulted from an intermolecular exchange of the N-terminal residues, which suggested that Trp[2] mediates the cis adhesive bond (*23*). Subsequent structures revealed either a disordered N terminus (*12, 24*) or the insertion of Trp[2] into its own hydrophobic pocket (*25*), which was suggested to induce a conformational change at a distinct adhesion site. The most recent crystal structure, including all five domains of C-cadherin (*26*), again showed a symmetric Trp[2] exchange between neighboring molecules, this time mediating a trans or intercellular contact. A number of alternative crystal contacts have also been proposed as adhesion interfaces, but no consensus has emerged for their physiological relevance.

[1]Skirball Institute of Biomolecular Medicine, [2]Department of Cell Biology, New York University School of Medicine, 540 First Avenue, New York, NY 10016, USA. [3]New York Structural Biology Center, 89 Convent Avenue, New York, NY 10027, USA.

*To whom correspondence should be addressed. E-mail: stokes@saturn.med.nyu.edu